

Solid-State Deracemization via Temperature Cycles in Continuous Operation: Model-Based Process Design

Brigitta Bodák and Marco Mazzotti*

Cite This: *Cryst. Growth Des.* 2022, 22, 1846–1856

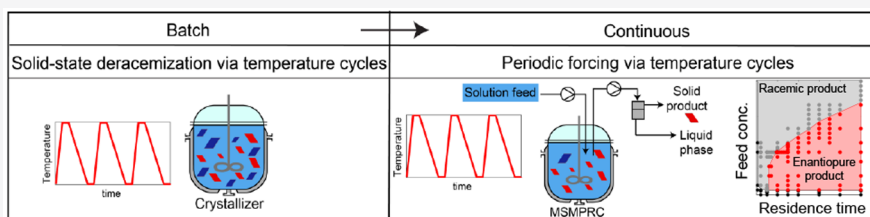
Read Online

ACCESS |

Metrics & More

Article Recommendations

Supporting Information



ABSTRACT: Solid-state deracemization via temperature cycles converts a racemic crystal mixture into an enantiopure product by periodic cycling of the temperature in the presence of a racemization catalyst. A continuous counterpart of this conventional batch-operated process is proposed that can be performed in mixed suspension mixed product removal crystallizers (MSMPRCs). More specifically, three different configurations are described to perform periodic forcing via temperature cycles, which differ from each other in the type of the feed and in the withdrawal system. We have developed a model by extending our recent population balance equation model of batch solid-state deracemization via temperature cycles, and we exploit this tool to analyze the start-up and periodic steady-state behavior. Moreover, we compare the performance of the different configurations based on the selected key performance indicators, namely, average periodic steady-state enantiomeric excess and productivity. The process with solution feed yields pure enantiomers, while the solid and suspension-fed process alternatives result in highly enantiomerically enriched crystals. We further design an MSMPRC cascade to overcome this purity limitation. This work discusses guidelines on how to transform the batch process of temperature cycles into a continuous operation, which enables stable, unattended operation and chiral crystal production with consistent product quality.

1. INTRODUCTION

Application of crystallization-based separation of racemic mixtures to obtain exclusively the enantiomer with the desired pharmacological effect is of high relevance in the pharmaceutical industry. Solid-state deracemization exploits liquid phase racemization to convert the undesired enantiomer to the preferred one, and it can be performed either via grinding a suspension of crystals^{1,2} or via applying temperature cycling^{3–9} (TC). In order to deracemize a chiral compound using the processes described here, three criteria need to be fulfilled: (i) it has to be a conglomerate-forming compound; (ii) a racemization reaction in solution must be feasible, to enable conversion between the two enantiomers; and (iii) an enantiomerically pure solid must be available to provide an enantiomerically enriched seed population.^{2,4,7,10} Though only 10% of organic chiral species are conglomerate-forming compounds, they are of increasing industrial interest.¹¹ Moreover, though deracemization is typically applied to compounds with a single chiral center, there are also examples related to molecules with multiple stereocenters.¹² In order to exploit the advantages of continuous operation,^{13,14} such as better quality consistency^{15,16} and a larger effective utilization time,¹⁷ continuous crystallization processes have been adapted for the separation of conglomerate-forming enantiomers.

Continuous preferential crystallization is a well-known choice,^{18,19} and it is the preferred method also in case racemization of enantiomers in the solution proves difficult.²⁰ If a racemization method is available, continuous Viedma ripening processes can be performed.^{21,22} The recent advances in implementing TC as an industrial process include its scale-up in coupled mixed-suspension vessels,²³ which were kept at low and high temperatures at a 50 mL scale; later, the scale-up was shown to be feasible in a 1 L vessel with the usage of a homogenizer.²⁴ Another step toward industrial application is based on the batch temperature cycling experiments carried out in a microwave reactor,²⁵ i.e., exploiting very fast heating and cooling rates, and its continuous alternative was presented by employing spatial thermal oscillations in a tubular flow millireactor.²⁶ In a recent work, the feasibility of performing continuous temperature cycles in a continuous tubular

Received: November 28, 2021

Revised: January 28, 2022

Published: February 9, 2022



crystallizer was demonstrated.²⁷ Nevertheless, to the best of our knowledge, application of periodic temperature cycles in mixed suspension mixed product removal crystallizers (MSMPRCs) for the purpose of solid-state deracemization has not been reported.

Yet, forced periodic operation of reactors is not uncommon in the field of chemical engineering. In case there are nonlinear effects in the process, the periodic modulations of the inputs can result in a better time-average performance than what one would obtain by operating the process in the steady state.²⁸ Thus, these periodic regimes are superior with respect to the optimal steady-state operation without periodic forcing, in terms of, for instance, selectivity and conversion.^{28–34} In this work, first, we present periodic forcing via temperature cycles (PFTC) in various single-stage MSMPRC schemes and in a multistage MSMPRC cascade configuration (section 2). Second, we extend the balance equations of batch temperature cycles to develop a model of PFTC that allows studying process dynamics and potential steady states (section 3). Then, we identify regions of operating conditions where enantiomerically pure crystals can be produced (section 4). Finally, the effect of selected process parameters (such as residence time, feed concentration, and cooling rate) on the performance indicators of the various configurations is comparatively assessed.

2. PROCESS DESIGN

Periodic forcing via temperature cycles is a solid-state deracemization process performed in a continuous crystallizer with liquid phase racemization and forced periodic operation of the temperature, aimed at producing enantiopure crystals of the desired enantiomer in a continuous manner. The crystallizer initially contains a saturated liquid with the racemization catalyst and a crystal population enriched in the desired enantiomer. The process is operated with continuous feed and continuous withdrawal, with forced periodic cycling of the temperature. In this work, three different types of feed are considered, namely, a solution feed, a solid feed, and a suspension feed, as indicated in Table 1.

Table 1. Summary of Configurations Presented to Perform Periodic Forcing via Temperature Cycles in Terms of Type of Feed and Recycle Utilized

configuration	type of feed	wet mill	recycle
base	solution	preferred, to generate particles	none
A	solid	optional	liquid
B	suspension	optional	none
cascade	solid	optional	liquid

In the base configuration, which is shown in Figure 1, a racemic solution constitutes the feed, while a suspension is continuously withdrawn from the crystallizer. This withdrawn suspension must contain crystals of the desired enantiomer only so as to obtain an enantiomerically pure product; thus, only this type of crystal should be present in the crystallizer. Therefore, a mechanism is required to continuously generate new crystals of only the desired enantiomer. Three mechanisms can form new crystals of the same handedness as the parent crystal in a continuous crystallizer, namely, (i) breakage, (ii) primary nucleation, and (iii) secondary nucleation. First, breakage is caused by for instance collisions between crystals and stirrer, or, alternatively, through the action of a milling unit when present.²¹ Then, primary nucleation can occur in this process only at conditions where the concentration of the undesired enantiomer is larger than that of the desired enantiomer (this is a constraint as we want to convert the former into the latter through the racemization reaction).³⁵ Therefore, primary nucleation of the desired enantiomer must be avoided, so as to avoid the nucleation of the undesired enantiomer; this can be avoided by keeping the supersaturation level below a (primary nucleation-) specific threshold. Finally, secondary nucleation occurs either by attrition, thus forming new crystals of the same handedness as the parent crystals or via other mechanisms^{36–40} that could in principle create nuclei of both enantiomers. The latter mechanism must clearly be prevented, namely, by keeping the supersaturation level below a (secondary nucleation-) specific threshold, which is even lower than the previous one. Such physical complexity is accounted for in the model by allowing for the formation of new nuclei of the desired enantiomer via secondary nucleation by attrition,⁴¹ as described in Table 2, and by constraining the simulations in such a way that the supersaturation with respect to the undesired enantiomer is kept below a given threshold, so as to avoid both its secondary and its primary nucleation. To model the mechanisms that occur in this process in a simple manner, both breakage and the formation of new nuclei of the desired enantiomer by secondary nucleation can be described as secondary nucleation via attrition by a simple breakage model,⁴¹ as Table 2 describes.

Alternatively, one can feed a racemic solid and convert it into enantiomerically pure solid, as in the case of configuration A illustrated in Figure 1. The suspension is withdrawn, and the crystalline product is obtained after filtration, while the liquid phase is completely recycled to the crystallizer from the filter, in order to keep the crystallizer volume constant.

Besides feeding either only solid or only liquid phase, feeding a suspension is also a viable option, as it is illustrated in

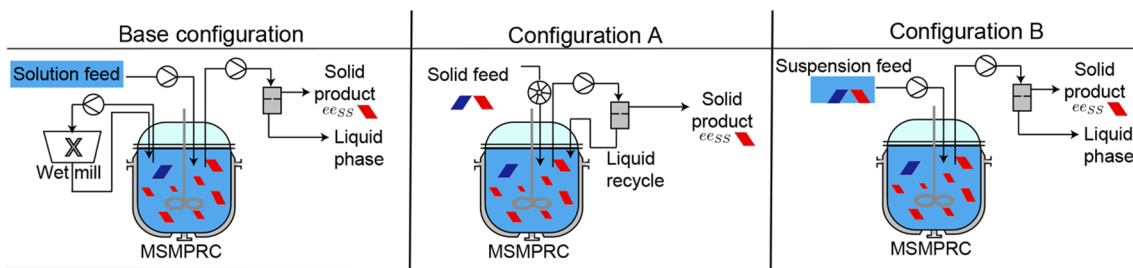


Figure 1. Crystallizer configurations to perform periodic forcing via a temperature cycles (PFTC) process: base configuration: solution-fed PFTC; configuration A: solid-fed PFTC with liquid recycle stream; configuration B: suspension-fed PFTC.

Table 2. Constitutive Equations of the PBE Model

Phenomena	Equation
Macroscopic solubility	$c_{\infty,i}(T) = q_{0,i} \exp\left(-\frac{q_{1,i}}{T}\right)$
Size-dependent growth/dissolution rate	$G_i(S_{\infty,i}, T, L) = \begin{cases} A_g(T) \sigma_i(S_{\infty,i}, T, L), & \sigma_i(S_{\infty,i}, T, L) > 0 \\ A_d(T) \sigma_i(S_{\infty,i}, T, L), & \sigma_i(S_{\infty,i}, T, L) \leq 0 \end{cases}$ with $\sigma_i(S_{\infty,i}, T, L) = \left(S_{\infty,i} - 1 - \frac{\alpha_{0,i}}{LT}\right)$, and $A_g(T) = k_{g,i} \exp\left(-\frac{E_{g,i}}{RT}\right)$, and $A_d(T) = k_{d,i} \exp\left(-\frac{E_{d,i}}{RT}\right)$
Racemization rate	$R_i(c_i, c_j, T) = k_{r0} \exp\left(-\frac{E_{r,i}}{RT}\right) (c_j - c_i)$ $i, j \in \{D, L\}$
Breakage in a wet suspension mill ²¹	
Daughter distribution	$g(L, \eta) = 3L^2 (2q + 1) \left(\frac{2}{\eta^3}\right)^{2q+1} \left(L^3 - \frac{\eta^3}{2}\right)^{2q}$
Breakage rate	$b(L) = k_b \left(\frac{L}{L_r}\right)$

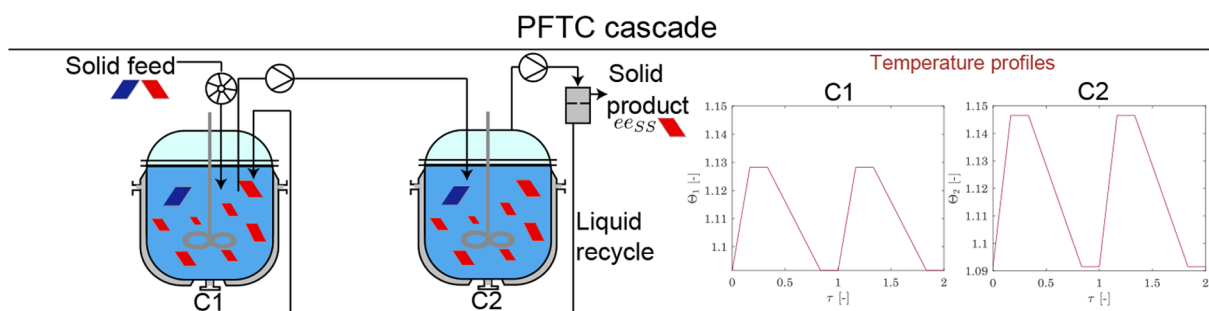


Figure 2. Solid-fed PFTC cascade.

Figure 1, process configuration B. Recycling of the liquid phase is not necessary in this configuration, as the crystallizer volume is kept constant by the continuous feed of the suspension. By feeding not only the racemic solid phase, but also a racemic solution to the MSMPRC, we reduce the asymmetry in the crystallizer, and thus less pure product and inferior process performance are expected.

In the configurations where the feed stream contains racemic crystals of both enantiomers (i.e., configurations A and B), the undesired enantiomer is introduced into the system in the solid phase, and thus an additional step is needed compared to the solution-fed process, namely, the dissolution of its crystals to enable racemization. Therefore, one can in principle expect inferior process performance in terms of productivity with respect to the base configuration; this is the first aspect in which the base configuration is expected to outperform configurations A and B. The second aspect is the lower enantiomeric purity of the product. It is an intrinsic property of a continuous mixed reactor that the product stream always contains the components of the feed stream, as a consequence of perfect mixing.⁴² It is therefore straightforward, based on chemical reaction engineering principles, that only for the configuration, which does not contain crystals of the undesired

enantiomer (i.e., base configuration), attaining complete enantiomeric purity is feasible. Note that the only feed strategy utilized as to date in continuous tubular temperature cycles experiments is the suspension feed,^{26,27} which is not the preferred feeding strategy in an MSMPR crystallizer, as it is expected to underperform the other two feed strategies. However, one could overcome the intrinsic limitation of continuous mixed flow reactors, e.g., by using a cascade of reactors. Moreover, in configurations A and B, as crystals are fed to the process, no crystal-generating unit such as the wet mill is required, which simplifies operation.

2.1. PFTC Cascade. Continuous crystallization is often carried out in multiple crystallizers, and thus we exploit this possibility also here by performing PFTC in a 2-MSMPC cascade. In this configuration, crystals are continuously fed to the first crystallizer, C1, from which a suspension is pumped to C2, as shown in Figure 2. The suspension leaving C2 is directly filtered, the solid is harvested, and the filtrate is completely recycled to C1. In both crystallizers, the temperature is cycled: the minimum temperature in both vessels is set to T_{\min} , and the temperature differences within a cycle, ΔT_1 and ΔT_2 , are set in C1 and C2 accordingly. Therefore, $T_{\max,2}$ is not necessarily equal to $T_{\max,1}$, and we adjust the heating/cooling

rates in C2 to obtain the same heating and cooling times, t_1 and t_3 , so as to synchronize temperature cycling in the two crystallizers. An additional case when $\Delta T_2 = 0$ is investigated as well, thus effectively mimicking the utilization of a dissolution vessel. In this cascade, the first crystallizer provides continuous seeding to the second reactor; these seeds are highly enriched in the desired enantiomer. Consequently, in the second reactor, at higher temperature than the first, the remaining small amount of crystals of the undesired enantiomer can dissolve. By operating in this way, small amounts of crystals of the desired enantiomer dissolve as well, but a high product purity can be achieved.

3. MATHEMATICAL MODEL

3.1. Constitutive Equations. The model of the continuous process is based on the batch variant, see section 3 in our previous work⁴³ for details. The thermodynamic and kinetic features of the model are accounted for through the constitutive equations, summarized in Table 2 for enantiomer i , ($i \in \{D, L\}$). It is worth noting that we are using a size-dependent solubility model, which enters into the definition of the driving force of both growth and dissolution.^{43–45}

Nucleation is not accounted for in the model, which is reasonable up to a system-specific supersaturation degree that is the threshold beyond which nucleation occurs. The values of the parameters presented here and their meaning are listed in Table 3. The particle size distribution (PSD) of enantiomer i ,

Table 3. Values of the Model Parameters^{43,45}

parameter	notation	value
activation energy of dissolution	$E_{d,i}$ [kJ kmol ⁻¹]	12000
activation energy of growth	$E_{g,i}$ [kJ kmol ⁻¹]	12000
activation energy of racemization	E_r [kJ kmol ⁻¹]	75000
breakage rate constant	k_b [s ⁻¹]	10 ⁻⁴
pre-exponential factor of dissolution	$k_{d,i}$ [$\mu\text{m s}^{-1}$]	200
pre-exponential factor of growth	$k_{g,i}$ [$\mu\text{m s}^{-1}$]	100
pre-exponential factor of racemization	$k_{r,i}$ [s ⁻¹]	10 ¹¹
surface shape factor	k_s [–]	π
volume shape factor	k_v [–]	$\pi/6$
universal gas constant	R [kJ kmol ⁻¹ K ⁻¹]	8.314
shape parameter of daughter distribution	q [–]	6
solubility parameter	$q_{0,i}$ [g g ⁻¹]	400
solubility parameter	$q_{1,i}$ [K]	2500
capillary length constant	α_0 [K m]	9.2×10^{-7}
crystal density	ρ_c [kg m ⁻³]	1300
solvent density	ρ_{solvent} [kg m ⁻³]	786

f_p is a function of particle size, L , and time, t . In our model, we define the PSD in units of the number of crystals per unit crystal length and unit mass of the solvent. The n th moment of the PSD is defined as

$$\phi_{n,i}(t) = \int_0^{+\infty} L^n f_i(L, t) dL \quad (1)$$

and the nominal supersaturation is $S_{\infty,i} = \frac{c_i}{c_{\infty,i}(T)}$. The solid phase enantiomeric excess of the D enantiomer, ee , is defined as the difference between the mass of the D enantiomer, m_D , and that of the L enantiomer, m_L , divided by their sum:

$$ee = \frac{m_D - m_L}{m_D + m_L} \quad (2)$$

The temperature profile is the typical profile applied in batch experiments,⁷ which is defined by periodic temperature cycling between T_{\min} and T_{\max} with $\Delta T = T_{\max} - T_{\min}$. Heating up the system to large temperature and thus removing all crystals of the undesired enantiomer in a single cycle are in general not possible because organic compounds remain stable only below a system-specific temperature threshold. The temperature cycle consists of four stages: a heating ramp with a time duration of t_1 , a high-temperature isothermal phase for t_2 , a cooling ramp for t_3 , and a low-temperature isothermal phase for t_4 . The reference time, t_r is equal to the duration of the entire temperature cycle, i.e., $t_r = t_1 + t_2 + t_3 + t_4$. When the cooling rate is varied, t_3 and t_r are adjusted accordingly. The operating conditions regarding temperature profile and scaling factors are reported in Table 4.

Table 4. Scaling Factors and Operating Conditions Kept Identical in Simulations^{43,45}

parameter	notation	value
reference size	L_r [μm]	100
reference time	t_r [s] ^a	3600
time of heating period	t_1 [s]	600
time of isothermal high T period	t_2 [s]	600
time of cooling period	t_3 [s] ^a	1800
time of isothermal low T period	t_4 [s]	600
minimum temperature	T_{\min} [K]	298
reference temperature	T_r [K]	273

^aThese parameters are adjusted when the cooling rate is varied.

3.2. Balance Equations. The assumptions made in developing the model of the continuous process are

- the residence time in the tubing, used for transfer of the solution and of the slurry, is negligible;
- the solution density is approximated by the solvent density, which does not change significantly within the temperature range considered;
- the suspension/solution entering the MSMPRC attains immediately the temperature of the receiving MSMPRC;
- the solid–liquid separation is considered to be perfect, i.e., without any loss of solvent;
- the mixing is perfect (i.e., the suspension is homogeneous), and there is no classification at withdrawal.

The equations are presented for the base configuration, and the derivation of the equations for other PFTC configurations shown in Figure 1 is straightforward and therefore only shown in the Supporting Information (see section S1). The system of equations consists of the population balance equations:

$$\frac{\partial f_i}{\partial t} + \frac{\partial(G_i(S_{\infty,i}, T, L)f_i)}{\partial L} = B_i(L, c_i, T) - D_i(L, c_i, T) - \frac{f_i}{t_{\text{res}}} \quad (3)$$

The first term on the left-hand side of eq 3 accounts for accumulation in the crystallizer of crystals of the enantiomer i between L and $L + \Delta L$, and the second term accounts for growth and dissolution; on the right-hand side of the equation, $B_i(L, c_i, T)$ and $D_i(L, c_i, T)$ are the birth and death terms due to breakage (or due to agglomeration, as in our previous work⁴³), whereas the last term accounts for the outlet stream, with residence time, t_{res} , defined as

$$t_{\text{res}} = \frac{m}{\dot{m}_{\text{out}}} \quad (4)$$

where m is the mass of solvent in the crystallizer, and \dot{m}_{out} is the mass flow rate of the outgoing stream, which is set to be identical to the mass flow rate of the feed. When the wet mill is included, we model the crystallizer and the mill as a single unit, and m represents the mass of solvent in this coupled unit. We note that in configuration A, the solid feed is characterized by its mass flow rate and its PSD, called \dot{M}_{in} and N_i , respectively, whereas in configuration B, $f_{\text{in},i}$ and \dot{m}_{in} are the PSD and the flow rate of the suspension feed, respectively.

The PBEs of eqs 3 are coupled with the following mass balances:

$$\frac{dc_i}{dt} + k_v \rho_c \frac{d\phi_{3,i}}{dt} = R_i(c_i, c_j, T) + \frac{c_{\text{in},i} - c_i}{t_{\text{res}}} - \frac{\phi_{3,i}}{t_{\text{res}}} k_v \rho_c, \quad i \in \{D, L\} \quad (5)$$

where $c_{\text{in},i}$ is the concentration of enantiomer i in the feed stream. The left-hand side of eq 5 accounts for accumulation, whereas the first term on the right-hand side accounts for the racemization reaction, and the second and third terms describe the inlet and outlet flows of the MSMPRC. The initial and boundary conditions are

$$\begin{aligned} f_i(L, 0) &= f_i^0(L) \\ f_i(0, t) &= 0 \\ c_i(0) &= c_{\text{in},i} \end{aligned} \quad (6)$$

where the initial supersaturation in the crystallizer is set equal to that of the feed solution.

The model equations are formulated assuming diluted conditions, i.e., of a suspension density less than 15%. In this case, choosing as basis the mother-liquor volume or the suspension volume is essentially the same, according to Randolph and Larson.⁴⁶ The case of higher suspension densities is beyond the scope of this work though the extension of the model is straightforward.⁴⁷

In practice, one transforms the equations into a system of nondimensional equations, as discussed in our previous work.⁴³ For details on the nondimensional system of equations, see section S2 in the Supporting Information; the rescaled quantities are reported in Table 5. Note that the initial PSDs are truncated Gaussian distributions, defined by their mean size (calculated based on the first and zeroth moments), $\bar{\lambda}_{i,0}$, and standard deviation, $\tilde{\sigma}_{i,0}$. In case crystals are fed, the feed PSDs are defined by their mean size and standard deviation, which we set to be identical to those of the initial PSD. Tables 7 and 8 summarize the initial conditions and the process parameters used in the simulations.

3.2.1. PFTC Cascade. The model equations for MSMPRC k , $k \in \{1, 2\}$, are presented in Table 6. The residence times are chosen to be equal in both crystallizers, i.e., $t_{\text{res},1} = t_{\text{res},2}$.

3.3. Solution of the PBEs. The PBEs of eqs 3 and 5 are solved using a high-resolution finite volume scheme with van Leer flux limiter and Godunov splitting.⁴⁸ The Godunov splitting is a fractional-step method consisting of two consecutive steps and gives a consistent approximation to the solution of the original equation.^{48–50} In the first step, the first subproblem, i.e., eq 3 with the right-hand side set to zero, is solved over a time step. The obtained PSD is used as initial

Table 5. Rescaling of the Model^{43,45}

rescaled quantities	notation	definition
rescaled PSD	\tilde{f}_i	$= f_i L_r$
rescaled third moment	$\tilde{\phi}_{3,i}$	$= \frac{\phi_{3,i}}{L_r^3}$
rescaled time	τ	$= \frac{t}{t_r}$
rescaled residence time	τ_{res}	$= \frac{t_{\text{res}}}{t_r}$
rescaled size	λ	$= \frac{L}{L_r}$
rescaled growth rate	\tilde{G}_i	$= \frac{t_r}{L_r} G_i$
rescaled racemization rate	$\kappa_{r,i}$	$= t_r \kappa_{r,i}$
rescaled breakage rate	K_{bg}	$= k_b t_r$
rescaled cooling rate	$\dot{\theta}_c$	$= \frac{d\theta}{d\tau} = \frac{dT}{dt} \frac{t_r}{T_r}$
rescaled feed constant	C	$= \frac{\dot{M}_{\text{in}}}{m} t_r$
rescaled solid feed PSD	\tilde{N}_i	$= L_r N_i$
rescaled suspension feed PSD	$\tilde{f}_{\text{in},i}$	$= L_r f_{\text{in},i}$

PSD to solve the second subproblem. In the second step, the PSD is updated by solving the second subproblem over a time step; i.e., the source term effects are computed. Thus, one alternates between the solution of growth/dissolution term and that of the source terms, namely, the breakage and the inlet and outlet flow terms. The model equations are discretized along both the space and the time coordinates, the result being an explicit time-marching algorithm or fully discrete scheme. The PBEs are coupled with mass balances, which are calculated by integration of eq 5 over a time step. See the Supporting Information Section S3 for details about the numerical algorithm.

3.4. Performance Indicators. Two important performance indicators for a deracemization process are the attained product purity and the productivity.

- Purity: The purity is defined to be the enantiomeric excess.
- Productivity: For continuous crystallization processes, the general productivity definition $P = \frac{\dot{m}_{\text{product}}}{m}$ is considered.^{19,22} The productivity for PFTC, by accounting for the enantiomeric excess of the product,⁴⁵ can be defined as

$$P = \frac{k_v \rho_c (\phi_{3,D,SS} - \phi_{3,L,SS})}{t_{\text{res}}} \quad (7)$$

where the SS subscript refers to the average value of the quantity within a single temperature cycle. Additionally, in the case of a PFTC cascade, t_{res} is defined as the sum of the residence times in the first and in the second reactor. In order to obtain the productivity values with the desired units, i.e., $\text{kg}^{-1} \text{h}^{-1}$, one needs to convert the model output accordingly.

4. RESULTS AND DISCUSSION

A batch process was simulated as a reference case, in which the solid phase is initially enriched in the D enantiomer (run 1 in Tables 7 and 8). Figure 3 shows the ee evolution as a function

Table 6. Model Equations of the PFTC Cascade Process

PBEs	$\frac{\partial f_{k,i}}{\partial t} + \frac{\partial (G_{k,i}(S_{\infty,k,i}, T_1, L) f_{k,i})}{\partial L} =$ $= B_{k,i}(L, c_{k,i}, T) - D_{k,i}(L, c_{k,i}, T_k) + \frac{\dot{M}_{k-1} N_i - \dot{m}_{out,k} f_{k,i}}{m_k}$ <p>where: $\dot{M}_{k-1} N_i = \begin{cases} \dot{M}_{in} N_i, & k = 1 \\ \dot{m}_{out,1} f_{1,i}, & k = 2 \end{cases}$</p>
mass balances	$\frac{dc_{k,i}}{dt} + k_v \rho_c \frac{d\phi_{3,k,i}}{dt} = R_{k,i}(c_{k,i}, c_{k,j}, T_k) + \text{inflow} - \text{outflow}$
initial and boundary conditions	$f_{k,i}(L, 0) = f_{k,i}(L)$ $f_{k,i}(0, t) = 0$ $c_{k,i}(0) = c_{k,\infty}(0)$

Table 7. Initial Conditions in the Simulations^a

run	configuration	ee_0 [-]	$\rho_{susp,0}$ [kg kg ⁻¹]	$\bar{\lambda}_{i,0}$ [-]	$\bar{\sigma}_{i,0}$ [-]	section
1	batch	0.40	0.10	1	0.05	3
2	base	0.40	0.10	1	0.05	3.1.1
3	base	0.40	0.10	1	0.05	3.1.2
4	base	0.40	0.10	1	0.05	3.1.2
5	base	0–1.00	0.10	1	0.05	3.1.3
6	base	0.40	0.04–0.12	1	0.05	3.1.3
7	A	0.40	0.10	1	0.05	3.2
8	A	0.40	0.10	1	0.05	3.2
9	B	0.40	0.10	1	0.05	3.3
10	cascade	0.40	0.10	1	0.05	3.4

^aNote that we set $\rho_{susp,0}$ and ee_0 in each simulation; $\bar{\phi}_{3,D,0}$ and $\bar{\phi}_{3,L,0}$ are not degrees of freedom.

of the number of cycles, τ , i.e., a dimensionless time; complete deracemization, i.e., $ee = 1$, is achieved after 16 cycles. For more details on the analysis of batch processes, the interested reader can see our previous work.⁴³

4.1. Solution-Fed PFTC. 4.1.1. Base Configuration. We analyze the dynamic behavior of the base case configuration, when supersaturated racemic solution is fed to the reactor ($c_{in,i} = 0.18 \text{ kg kg}^{-1}$, run 2). The periodic steady-state condition for an MSMPR reactor involving crystallization has been recently defined as the state of the system, which maintains itself despite transitory effects caused by periodic disturbances or periodic forcing.⁵¹ Thus, a periodic steady state is defined as the time-average computed between the maximum and minimum values obtained periodically at steady state. The enantiomeric excess as a function of the normalized time, τ , is

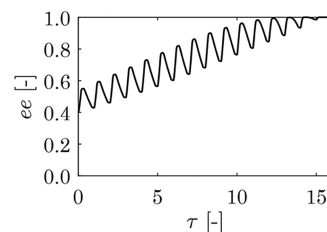


Figure 3. Batch process: evolution of the ee as a function of nondimensional time (run 1).

shown in Figure 4a (where the inset is a magnification, the time averaged value is shown as a black solid line, and its instantaneous value appears as a green-shaded region). The evolution of the enantiomeric excess during the start-up phase is similar as in batch temperature cycles; i.e., the ee increases during the heating phase and the isothermal holding phase at high temperature, and then it decreases during the cooling phase and the isothermal holding phase at low temperature. At steady state, enantiopurity is reached (i.e., $ee_{SS} = 1$). The third moment evolution of each enantiomer, which is proportional to the crystal mass, is shown in Figure 4b. The time averaged mass of the D enantiomer (red solid line) and that of the L enantiomer (blue solid line) increase steeply due to the large initial and feed concentration, and both crystals grow, as illustrated by the gray dashed lines representing the time averaged total mass of crystals. Then, the mass of both populations decreases, which is followed by an increase in the crystal mass of D enantiomers and a gradual decrease of the crystal mass of L enantiomer. Finally, the crystals populations approach an average periodic steady-state value, which is 0 for

Table 8. Process Parameters Varied in the Simulations^a

run	τ_{res} [-]	ΔT [K]	$\dot{\theta}_c \times 10^2$ [-]	$\dot{M}_{in}/\dot{m}_{out}$ [-]	mill [-]	ee_{in} [-]	$\bar{\lambda}_{in,i}$ [-]	$\bar{\sigma}_{in,i}$ [-]	ρ_{in} [-]	$c_{in,i}$ [kg kg ⁻¹]
1	batch	10	7.33							
2	15	10	7.33		M					0.18
3	2–50	10	7.33		M					0.09–0.27
4	15	10	7.33–20.2		M					0.18
5	15	10	7.33		M					0.18
6	15	10	7.33		M					0.18
7	10–100	10	7.33	0.10	–/M	0	1	0.05		
8	50	10	7.33	0.05–0.35	M	0	1	0.05		
9	50	10	7.33	$\dot{m}_{in} = \dot{m}_{out}$		0	1	0.05	0.017–0.150	0.09
10	50	$\Delta T_1 = 10$ $\Delta T_2 = 0; 15$	$\dot{\theta}_{c,1} = 7.33$ $\dot{\theta}_{c,2}^*$	2.0 2.0		0 0	1 1	0.05 0.05		

^aVaried to have t_1 and t_3 values as in the first MSMPRC.

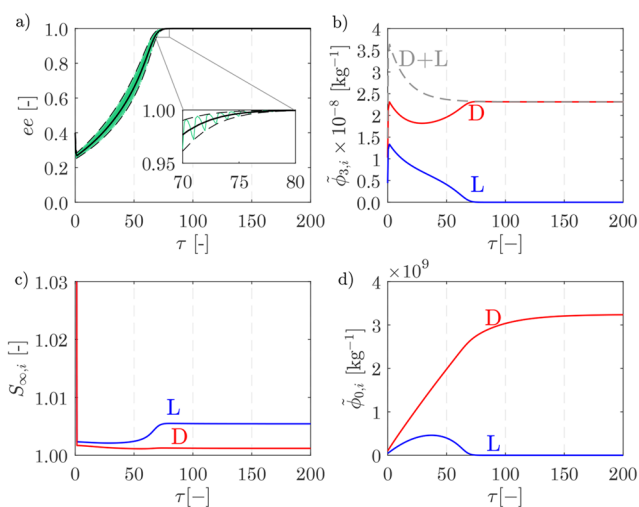


Figure 4. Transient and steady-state behavior of the solution-fed PFTC process (base configuration, run 2). (a) The evolution of the ee along the process: the instantaneous ee is shown with a green solid line, the average ee during the cycles is plotted with a black solid line. The black dashed lines present the upper and lower periodic boundaries. (b) The time averaged value of the rescaled third moment during the process for the D (red lines) and L (blue lines) enantiomers, and their sum (gray dashed line), respectively. (c) The supersaturation profiles during the cycles for the D (red lines) and the L (blue lines) enantiomers. (d) The evolution of the average number of particles of D (red solid line) and L (blue solid line).

the L enantiomer, thus confirming that only the enantiopure D enantiomer crystals remain. The average supersaturation of the L enantiomer is larger than that of D; thus, racemization occurs in the desired direction, as Figure 4c shows with blue and red lines, respectively. Figure 4d shows that the rescaled zeroth moment, i.e., the number of particles of the D enantiomer at steady state, is larger than its initial value, as a consequence of milling, and that of L particles reaches 0.

4.1.2. Effect of Operating Conditions. A simulation study has been performed by varying the residence time and the feed concentration in order to investigate their effect on the achievable steady state and on the process performance.

First, we analyze the effect of the residence time, τ_{res} , on the average steady-state enantiomeric excess, ee_{SS} , and on the

productivity, P_{SS} , as illustrated in Figure 5a (run 3). When the residence time is very low, the crystals get washed out, resulting in a trivial steady state (white zone and black symbols in Figure 5a). At low residence times (i.e., $1 \leq \tau_{\text{res}} < 9.8$), a steady state with racemic crystal composition is achieved (i.e., $ee_{\text{SS}} = 0$, gray zone and symbols in Figure 5a). At larger residence times (i.e., $9.8 \leq \tau_{\text{res}}$), only D crystals are obtained (i.e., $ee_{\text{SS}} = 1$, red zone and symbols in Figure 5a). However, one can notice that the productivity decreases with increasing residence time. Thus, a threshold residence time exists, below which the deracemization capacity of the process is too low to show for complete deracemization, while at this value, the deracemization capacity is optimal. Then, further increasing τ_{res} results in unutilized deracemization capacity.

Second, Figure 5b shows the attainable steady states (or ee_{SS}) as a function of both τ_{res} and the feed concentration, $c_{\text{in},i}$. When the residence time is kept constant (i.e., we are moving vertically along the plane), we can observe that at low $c_{\text{in},i}$ the trivial steady state is obtained (black symbols). When $c_{\text{in},i}$ increases, D enantiomers are obtained at steady state (i.e., $ee_{\text{SS}} = 1$, red symbols). In the high feed concentration region, a racemic steady state is reached (i.e., $ee_{\text{SS}} = 0$, gray symbols). It is trivial that the simulated points of Figure 5a are located along a vertical line at $c_{\text{in},i} = 0.18$ in Figure 5b. It is remarkable that $0 < ee_{\text{SS}} < 1$ is never obtained. Note that a steady state where pure enantiomeric crystals are obtained is not achievable at low residence times.

In order to further explore the effect of operating conditions, we performed simulations by varying the normalized cooling rate between the minimum value $\theta_c = 0.073$ and the maximum value $\theta_c = 0.202$ (run 4, the range corresponding to $0.33\text{--}0.50 \text{ K min}^{-1}$ utilized in batch experiments^{4,7,52}), and the ee_{SS} reaches 1 in all simulations. Thus, the continuous process is not sensitive to changes in the cooling rate in the investigated range, contrary to the batch process.⁴³

4.1.3. Effect of Initial Conditions. By choosing the initial conditions carefully, one can shorten the time to reach the periodic steady state. Figure 6a (run 5) shows that the ee_{SS} (green symbols) is not dependent on the ee_0 , while the time to reach the periodic steady state, τ_{SS} (blue symbols), becomes significantly shorter with increasing ee_0 , as expected. By running simulations at varying initial suspension density, ρ_0 , the independence of the ee_{SS} from the initial values has been

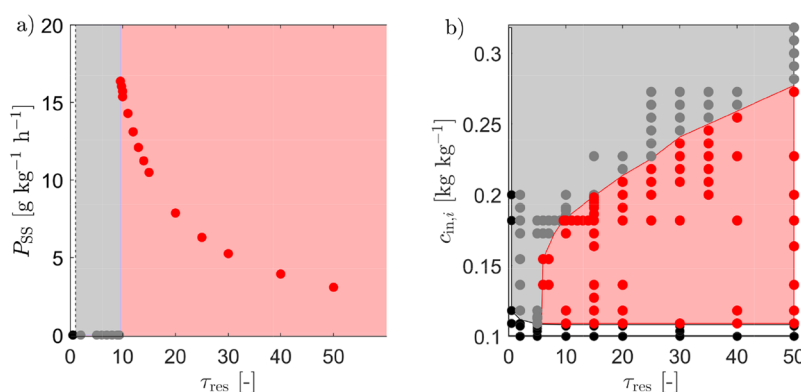


Figure 5. (a) Effect of the residence time, τ_{res} , on the productivity, P_{SS} , in the solution-fed process (base configuration, run 3, at $c_{\text{in},i} = 0.18 \text{ kg kg}^{-1}$); (b) map of steady-state outcomes spanned by the feed concentration, $c_{\text{in},i}$, and by τ_{res} . The symbols represent the steady-state value of the system; red symbol corresponds to a case with D enantiomer product, gray symbols mark the case when racemic crystals are obtained, and black symbols represent a steady state without crystals, i.e., a trivial steady state.

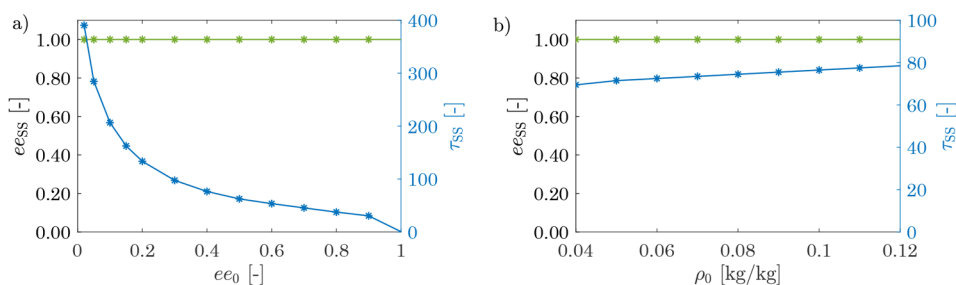


Figure 6. (a) Average steady-state enantiomeric excess, ee_{SS} (green stars, left), and start-up time, τ_{SS} (blue stars, right), as a function of initial enantiomeric excess, ee_0 , in the solution-fed process (base configuration, run 5). (b) Effect of initial suspension density on the ee_{SS} (green stars, left) and τ_{SS} (blue stars, right), are shown (base configuration, run 6).

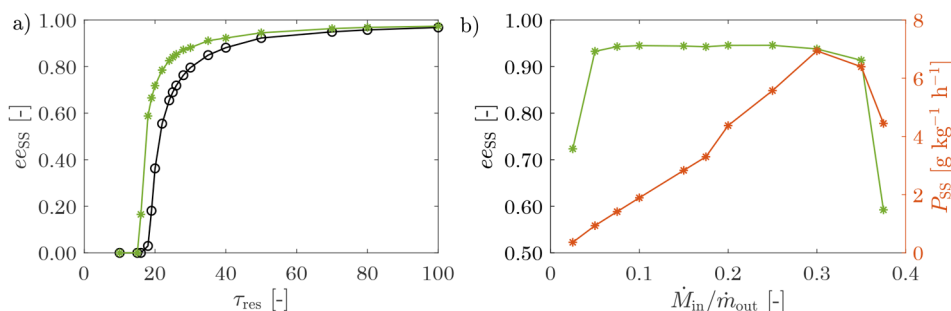


Figure 7. (a) Effect of the residence time, τ_{res} on the average steady-state enantiomeric excess, ee_{SS} , without and with milling indicated by open circles and stars, respectively; (b) effect of the ratio of the solid feed rate and of the suspension withdrawal rate, $\dot{M}_{in}/\dot{m}_{out}$ on ee_{SS} (green stars, left axis), and on the productivity, P_{SS} (red stars, right axis), in the solid-fed process (configuration A, run 8).

further confirmed, as Figure 6b shows (run 6). One can also observe that increasing ρ_0 , also τ_{SS} increases, as expected, due to the larger number of crystals of the undesired enantiomer that needs to be deracemized in the process.

4.2. Solid-Fed PFTC. We have performed simulations in configuration A (i.e., by feeding racemic crystals), and we have varied the residence time (run 7) in order to investigate its effect on the ee_{SS} . Figure 7a shows that by increasing the residence time, the ee_{SS} increases (black circles). However, the ee_{SS} never reaches 1, as expected, based on the rationale given in section 2. One can notice that given the same residence time, the ee_{SS} can be higher when one utilizes a mill (green symbols), as the mill comminutes the particles of the undesired enantiomer that are not yet dissolved in the cycles, thus accelerating their dissolution.

Moreover, increasing the ratio of the solid feed rate with respect to the suspension withdrawal rate, $\dot{M}_{in}/\dot{m}_{out}$, is a potential way to increase the productivity (configuration A, run 8). Interestingly, the ee_{SS} is low at low feed rates, as the surface available for growth of the desired enantiomer is not enough to compensate for that of the withdrawn crystals (Figure 7a, left axis, green symbols). Then, by increasing the solid feed rate, the ee_{SS} reaches a maximum, and then it decreases (the feeding rate of the racemic solid is too high with respect to the rate of deracemization). Figure 7b illustrates that the average steady-state productivity, P_{SS} , obviously increases with an increasing feed rate (Figure 7b, right axis, red stars), reaches a maximum, and then decreases, as smaller (larger) amounts of target (undesired) enantiomer are produced. Thus, an optimal feed rate exists, at which the deracemizing capacity of the suspension in the crystallizer is exploited to the maximum.

4.3. Suspension-Fed PFTC. In this section, the suspension-fed continuous process (configuration B) is analyzed.

First, we compare the performance of configuration B ($\rho_{in} = 0.100 \text{ kg kg}^{-1}$, run 9) with that of the solid-fed variant (configuration A, run 7) at an identical residence time ($\tau_{res} = 50$). Note that in both simulations, the same amount of crystals are fed per unit time, but in configuration A, only solid is fed, while in configuration B, the solid is suspended in a saturated solution (therefore, the liquid phase is not recycled after filtration). The suspension-fed process reaches $ee_{SS} = 0.88$ (configuration B) versus $ee_{SS} = 0.92$ for the solid-fed process (configuration A). The corresponding productivities are $1.30 \text{ g kg}^{-1} \text{ h}^{-1}$ and $1.84 \text{ g kg}^{-1} \text{ h}^{-1}$, respectively. It is therefore preferable to feed the crystals only, without a solution, as expected. In the case of feeding a suspension, the liquid composition is racemic; in the solid-fed process, the solution is recycled; thus, it is not racemic, and thus it provides a larger driving force for the racemization, and therefore it enables faster deracemization.

Second, we analyze the effect of varying feed suspension density on the steady state (run 9). Figure 8 shows that low values of ρ_{in} result in a racemic product, while with increasing values of ρ_{in} , the corresponding values of ee_{SS} (black triangles) and the P_{SS} (red circles) increase as well. Note that at low feed suspension densities, the crystal generation in the MSMPCR, namely, the solid feed, is not sufficient to operate the process with reasonable productivity. Therefore, a minimum feed suspension density exists, above which the configuration B is able to produce crystals while achieving reasonable levels of ee_{SS} and P_{SS} .

4.4. PFTC Cascade. In the solid-fed configuration, the ee_{SS} never reached 1. Therefore, we have explored whether running

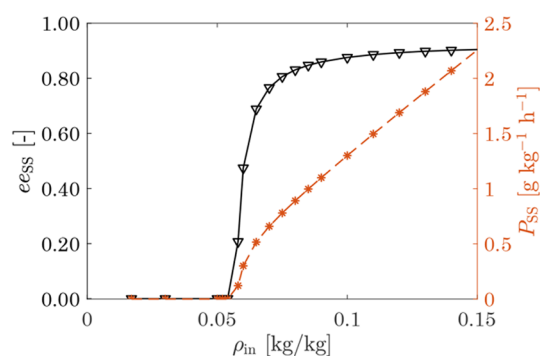


Figure 8. Effect of feed suspension density, ρ_{in} , on the average steady-state enantiomeric excess, ee_{SS} (left, black triangles) and on the average steady-state productivity, P_{SS} (right, red circles), in the suspension-fed process (configuration B, run 9).

this process in a cascade enables reaching complete deracemization, and thus two PFTC cascade simulations were carried out (run 10). In all simulations, the temperature profile in C1 was set to be the temperature cycle with $\Delta T_1 = 10$ K, i.e., the same amplitude as in previous simulations. In C2, we explored two different options. In the first case, the maximum temperature difference within a cycle was large: $\Delta T_2 = 15$ K. In the second case, the temperature is constant at high temperature, $T_{max,2}$. In both cases, as Table 9 shows,

Table 9. Initial Conditions in the Simulations^a

	$\Delta T_1 = 10$ K, $\Delta T_2 = 15$ K	$\Delta T_1 = 10$ K, $T_2 = \text{const} = T_{max,2}$
ee_{SS}	1.00	1.00
P_{SS}	1.01	1.02

^aNote that we set $\rho_{susp,0}$ and ee_0 in each simulation; $\tilde{\phi}_{3,D0}$ and $\tilde{\phi}_{3,L0}$ are not degrees of freedom.

enantiopure D crystals with similar productivities are obtained. C2 acts as a temperature cycling dissolution vessel in the first case, and it is a dissolution vessel at constant temperature in the second case. The minimum temperature of the dissolution vessel that enables complete dissolution of the crystals of the undesired enantiomer depends on the dissolution rates of specific compounds, and it also needs to be selected as a function of residence times.

5. CONCLUSIONS

Novel mixed-suspension mixed product removal crystallizer-based configurations have been proposed in this work for the first time to perform periodic forcing via temperature cycles. By extending our model of batch deracemization via temperature cycles, the population balance equation based model of each continuous configuration has been developed to perform model-based investigation of this process. An efficient numerical algorithm has been implemented that allowed us to perform process analysis. Although the kinetic parameters used in this work are reasonable in terms of their order of magnitude, they represent a hypothetical compound. Nevertheless, we have demonstrated that the developed PBE-based modeling platform is essential, as it enables one to design novel processes and to develop valuable guidelines for their implementation.

First, a base configuration, where the feed is a solution, has been proposed; where a racemic solution is fed, the solid acts

as seed, and the steady state is independent of the initial conditions, thus resulting in a robust process. It has been shown that among the operating parameters, the residence time and the feed concentration have the largest impact on the process performance, as they define the region where an enantiopure product or racemic product can be obtained at steady state. The limitations of this process are that the target compound should be stable at a high temperature at which the feed solution is prepared, and the process has to be operated at such conditions, at which nucleation of the undesired enantiomer does not occur.²²

If these conditions cannot be fulfilled, alternatively, the solid-fed configuration can be utilized. This second configuration (i.e., configuration A) was found to produce enantiomerically highly enriched crystals, which can be achieved by tuning the operating parameters, namely, the residence time and the solid feed rate. Finally, a third alternative, a suspension-fed configuration (i.e., configuration B) was shown to underperform the solid-fed configuration.

The purity limitation of the solid-fed configuration has been overcome by the addition of a second, dissolution vessel, which can be operated either by large temperature ramps or by holding it at high temperature. The potential advantage of such a dissolution vessel was suggested in the literature for continuous resolution of conglomerate-forming compounds;²¹ however, it has been proven in this work via simulations that an enantiopure product can indeed be achieved in such configuration.

Our two final take-home messages are as follows. First, we have been able to show that batch-wise deracemization via temperature cycles can be made continuous through the configurations presented here. This has obvious advantages in terms of stability of operation and of product consistency. Second, a clear disadvantage with respect to batch-wise temperature cycles is the intrinsic difficulty in continuous processes to correct for the possible occurrence of nucleation of the undesired enantiomer, which could be overcome with periodic forcing of the temperature. Thus, summarizing, with this work and the companion literature from this group, we have provided a family of deracemization processes for conglomerate forming systems, which collectively provide a number of very useful alternative approaches, and we have thoroughly comparatively assessed their merits.

■ ASSOCIATED CONTENT

SI Supporting Information

The Supporting Information is available free of charge at <https://pubs.acs.org/doi/10.1021/acs.cgd.1c01398>.

Model equations of various PFTC configurations, the nondimensional model equations, and details on the numerical algorithm (PDF)

■ AUTHOR INFORMATION

Corresponding Author

Marco Mazzotti – Institute of Energy and Process Engineering, ETH Zurich, 8092 Zurich, Switzerland; orcid.org/0000-0002-4948-6705; Phone: +41 44 632 24 56;

Email: marco.mazzotti@ipe.mavt.ethz.ch; Fax: +41 44 632 11 41

Author

Brigitta Bodák – Institute of Energy and Process Engineering, ETH Zurich, 8092 Zurich, Switzerland;  orcid.org/0000-0002-1979-9815

Complete contact information is available at:
<https://pubs.acs.org/10.1021/acs.cgd.1c01398>

Notes

The authors declare no competing financial interest.

ACKNOWLEDGMENTS

B.B and M.M. are grateful for the funding received as part of the CORE project (October 2016–September 2020) from the European Union's Horizon 2020 Research and Innovation Programme under the Marie Skłodowska-Curie Grant Agreement No. 722 456 CORE ITN. This project has also received funding from the European Research Council (ERC) under the European Unions Horizon 2020 Research and Innovation Programme under Grant Agreement No. 788 607.

REFERENCES

- (1) Viedma, C. Chiral symmetry breaking during crystallization: Complete chiral purity induced by nonlinear autocatalysis and recycling. *Phys. Rev. Lett.* **2005**, *94*, 3–6.
- (2) Noorduyn, W. L.; van Enkevort, W. J. P.; Meekes, H.; Kaptein, B.; Kellogg, R. M.; Tully, J. C.; McBride, J. M.; Vlieg, E. The Driving Mechanism Behind Attrition-Enhanced Deracemization. *Angew. Chem.* **2010**, *122*, 8613–8616.
- (3) Viedma, C. Chiral symmetry breaking and complete chiral purity by thermodynamic-kinetic feedback near equilibrium: implications for the origin of biochirality. *Astrobiology* **2007**, *7*, 312–319.
- (4) Suwannasang, K.; Flood, A. E.; Rougeot, C.; Coquerel, G. Using programmed heating-cooling cycles with racemization in solution for complete symmetry breaking of a conglomerate forming system. *Cryst. Growth Des.* **2013**, *13*, 3498–3504.
- (5) Li, W. W.; Spix, L.; De Reus, S. C.; Meekes, H.; Kramer, H. J.; Vlieg, E.; Ter Horst, J. H. Deracemization of a racemic compound via its conglomerate-forming salt using temperature cycling. *Cryst. Growth Des.* **2016**, *16*, 5563–5570.
- (6) Suwannasang, K.; Flood, A. E.; Rougeot, C.; Coquerel, G. Use of Programmed Damped Temperature Cycles for the Deracemization of a Racemic Suspension of a Conglomerate Forming System. *Org. Process Res. Dev.* **2017**, *21*, 623–630.
- (7) Breveglieri, F.; Maggioni, G. M.; Mazzotti, M. Deracemization of NMPA via Temperature Cycles. *Cryst. Growth Des.* **2018**, *18*, 1873–1881.
- (8) Maggioni, G. M.; Fernández-Ronco, M. P.; Van Der Meijden, M. W.; Kellogg, R. M.; Mazzotti, M. Solid state deracemization of two imine-derivatives of phenylglycine derivatives via high-pressure homogenisation and temperature cycles. *CrystEngComm* **2018**, *20*, 3828–3838.
- (9) Oketani, R.; Hoquante, M.; Brandel, C.; Cardinael, P.; Coquerel, G. Practical Role of Racemization Rates in Deracemization Kinetics and Process Productivities. *Cryst. Growth Des.* **2018**, *18*, 6417–6420.
- (10) Noorduyn, W. L.; Meekes, H.; Van Enkevort, W. J.; Kaptein, B.; Kellogg, R. M.; Vlieg, E. Enantioselective symmetry breaking directed by the order of process steps. *Angewandte Chemie - International Edition* **2010**, *49*, 2539–2541.
- (11) Jacques, J.; Collet, A. *Enantiomers, Racemates, and Resolutions*; J. Wiley and Sons, Inc.: Hoboken, NJ, USA, 1981.
- (12) Engwerda, A. H.; Mertens, J. C.; Tinnemans, P.; Meekes, H.; Rutjes, F. P.; Vlieg, E. Solid-Phase Conversion of Four Stereoisomers into a Single Enantiomer. *Angewandte Chemie - International Edition* **2018**, *57*, 15441–15444.
- (13) Fisher, A. C.; Lee, S. L.; Harris, D. P.; Buhse, L.; Kozlowski, S.; Yu, L.; Kopcha, M.; Woodcock, J. Advancing pharmaceutical quality: An overview of science and research in the U.S. FDA's Office of Pharmaceutical Quality. *Int. J. Pharm.* **2016**, *515*, 390–402.
- (14) Burcham, C. L.; Florence, A. J.; Johnson, M. D. Continuous manufacturing in pharmaceutical process development and manufacturing. *Annu. Rev. Chem. Biomol. Eng.* **2018**, *9*, 253–281.
- (15) Quon, J. L.; Zhang, H.; Alvarez, A.; Evans, J.; Myerson, A. S.; Trout, B. L. Continuous crystallization of Aliskiren hemifumarate. *Cryst. Growth Des.* **2012**, *12*, 3036–3044.
- (16) Yang, Y.; Nagy, Z. K. Advanced control approaches for combined cooling/antisolvent crystallization in continuous mixed suspension mixed product removal cascade crystallizers. *Chem. Eng. Sci.* **2015**, *127*, 362–373.
- (17) Schaber, S. D.; Gerogiorgis, D. I.; Ramachandran, R.; Evans, J. M.; Barton, P. I.; Trout, B. L. Economic analysis of integrated continuous and batch pharmaceutical manufacturing: A case study. *Ind. Eng. Chem. Res.* **2011**, *50*, 10083–10092.
- (18) Vetter, T.; Burcham, C. L.; Doherty, M. F. Separation of conglomerate forming enantiomers using a novel continuous preferential crystallization process. *AIChE J.* **2015**, *61*, 2810–2823.
- (19) Majumder, A.; Nagy, Z. K. A comparative study of coupled preferential crystallizers for the efficient resolution of conglomerate-forming enantiomers. *Pharmaceutics* **2017**, *9*, 55.
- (20) Fogassy, E.; Nógrádi, M.; Kozma, D.; Egri, G.; Pálóvics, E.; Kiss, V. Optical resolution methods. *Organic and Biomolecular Chemistry* **2006**, *4*, 3011–3030.
- (21) Köllges, T.; Vetter, T. Model-based analysis of continuous crystallization/reaction processes separating conglomerate forming enantiomers. *Cryst. Growth Des.* **2017**, *17*, 233–247.
- (22) Köllges, T.; Vetter, T. Design and Performance Assessment of Continuous Crystallization Processes Resolving Racemic Conglomerates. *Cryst. Growth Des.* **2018**, *18*, 1686–1696.
- (23) Suwannasang, K.; Flood, A. E.; Coquerel, G. A Novel Design Approach to Scale Up the Temperature Cycle Enhanced Deracemization Process: Coupled Mixed-Suspension Vessels. *Cryst. Growth Des.* **2016**, *16*, 6461–6467.
- (24) Steendam, R. R.; Ter Horst, J. H. Scaling Up Temperature Cycling-Induced Deracemization by Suppressing Nonstereoselective Processes. *Cryst. Growth Des.* **2018**, *18*, 3008–3015.
- (25) Cameli, F.; Xiouras, C.; Stefanidis, G. D. Intensified deracemization via rapid microwave-assisted temperature cycling. *CrystEngComm* **2018**, *20*, 2897–2901.
- (26) Cameli, F.; Xiouras, C.; Stefanidis, G. D. High-throughput on demand access of single enantiomers by a continuous flow crystallization process. *CrystEngComm* **2020**, *22*, 3519–3525.
- (27) Neugebauer, P.; Triebel, A.; Gruber-Woelfler, H. Complete chiral resolution in a continuous flow crystallizer with recycle stream. *Journal of Flow Chemistry* **2021**, *11*, 483–493.
- (28) Nikolić, D.; Seidel-Morgenstern, A.; Petkovska, M. Nonlinear frequency response analysis of forced periodic operation of non-isothermal CSTR using single input modulations. Part I: Modulation of inlet concentration or flow-rate. *Chem. Eng. Sci.* **2014**, *117*, 71–84.
- (29) Douglas, J. M.; Rippin, D. W. Unsteady state process operation. *Chem. Eng. Sci.* **1966**, *21*, 305–315.
- (30) Bailey, J. E. Periodic operation of chemical reactors: A review. *Chem. Eng. Commun.* **1974**, *1*, 111–124.
- (31) Sterman, L. E.; Erik Ydstie, B. Unsteady-state multivariable analysis of periodically perturbed systems. *Chem. Eng. Sci.* **1990**, *45*, 737–749.
- (32) Marković, A.; Seidel-Morgenstern, A.; Petkovska, M. Evaluation of the potential of periodically operated reactors based on the second order frequency response function. *Chem. Eng. Res. Des.* **2008**, *86*, 682–691.
- (33) Nikolić, D.; Seidel-Morgenstern, A.; Petkovska, M. Nonlinear frequency response analysis of forced periodic operation of non-isothermal CSTR with simultaneous modulation of inlet concentration and inlet temperature. *Chem. Eng. Sci.* **2015**, *137*, 40–58.
- (34) Nikolić, D.; Seidel-Morgenstern, A.; Petkovska, M. Periodic Operation with Modulation of Inlet Concentration and Flow Rate.

Part I: Nonisothermal Continuous Stirred-Tank Reactor. *Chem. Eng. Technol.* **2016**, *39*, 2020–2028.

(35) Denk, E. G.; Botsaris, G. D. Fundamental studies in secondary nucleation from solution. *J. Cryst. Growth* **1972**, *13–14*, 493–499.

(36) Qian, R. Y.; Botsaris, G. D. Nuclei breeding from a chiral crystal seed of NaClO₃. *Chem. Eng. Sci.* **1998**, *53*, 1745–1756.

(37) Cui, Y.; Stojakovic, J.; Kijima, H.; Myerson, A. S. Mechanism of Contact-Induced Heterogeneous Nucleation. *Cryst. Growth Des.* **2016**, *16*, 6131–6138.

(38) Xu, S.; Wang, Y.; Hou, Z.; Chuai, X. Overview of secondary nucleation: From fundamentals to application. *Ind. Eng. Chem. Res.* **2020**, *59*, 18335–18356.

(39) Bosetti, L.; Ahn, B.; Mazzotti, M. Secondary Nucleation by Interparticle Energies. I. Thermodynamics. *Cryst. Growth Des.* **2022**, *22*, 87–97.

(40) Ahn, B.; Bosetti, L.; Mazzotti, M. Secondary Nucleation by Interparticle Energies. II. Kinetics. *Cryst. Growth Des.* **2022**, *22*, 74–86.

(41) Bosetti, L.; Mazzotti, M. Population Balance Modeling of Growth and Secondary Nucleation by Attrition and Ripening. *Cryst. Growth Des.* **2020**, *20*, 307–319.

(42) Levenspiel, O. *Chemical Reaction Engineering*; John Wiley & Sons: New York, NY, 2007.

(43) Bodák, B.; Maggioni, G. M.; Mazzotti, M. Population-Based Mathematical Model of Solid-State Deracemization via Temperature Cycles. *Cryst. Growth Des.* **2018**, *18*, 7122–7131.

(44) Iggland, M.; Mazzotti, M. A population balance model for chiral resolution via Viedma ripening. *Cryst. Growth Des.* **2011**, *11*, 4611–4622.

(45) Bodák, B.; Maggioni, G. M.; Mazzotti, M. Effect of Initial Conditions on Solid-State Deracemization via Temperature Cycles: A Model-Based Study. *Cryst. Growth Des.* **2019**, *19*, 6552–6559.

(46) Randolph, A. D.; Larson, M. A. *Chemical Reaction Engineering*; Academic Press: San Diego, CA, 1988.

(47) Li, J.; Trout, B. L.; Myerson, A. S. Multistage Continuous Mixed-Suspension, Mixed-Product Removal (MSMPR) Crystallization with Solids Recycle. *Org. Process Res. Dev.* **2016**, *20*, 510–516.

(48) LeVeque, R. J. *Finite Vol. Methods for Hyperbolic Problems*; Cambridge University Press: Cambridge, UK, 2002.

(49) Gunawan, R.; Fusman, I.; Braatz, R. D. High resolution algorithms for multidimensional population balance equations. *AIChE J.* **2004**, *50*, 2738–2749.

(50) Gunawan, R.; Fusman, I.; Braatz, R. D. Parallel High-Resolution Finite Volume Simulation of Particulate Processes. *AIChE J.* **2008**, *54*, 1449–1458.

(51) Powell, K. A.; Saleemi, A. N.; Rielly, C. D.; Nagy, Z. K. Periodic steady-state flow crystallization of a pharmaceutical drug using MSMPR operation. *Chemical Engineering and Processing: Process Intensification* **2015**, *97*, 195–212.

(52) Oketani, R.; Hoquante, M.; Brandel, C.; Cardinael, P.; Coquerel, G. Resolution of an Atropisomeric Naphthamide by Second-Order Asymmetric Transformation: A Highly Productive Technique. *Org. Process Res. Dev.* **2019**, *23*, 1197–1203.